Research Article

NEURAL REGENERATION RESEARCH
www.nrronline.org

Electrodeposition of chitosan/graphene oxide conduit to enhance peripheral nerve regeneration

Ya-Nan Zhao[1, 2, #], Ping Wu[1, #], Zi-Yuan Zhao[3], Fei-Xiang Chen[1], Ao Xiao[1], Zhi-Yi Yue[1], Xin-Wei Han[2], Yong Zheng[1, *], Yun Chen[1, *]

https://doi.org/10.4103/1673-5374.344836

Date of submission: March 31, 2021

Date of decision: October 22, 2021

Date of acceptance: April 14, 2022

Date of web publication: June 6, 2022

From the Contents

Graphical Abstract

The electrodeposited chitosan/graphene oxide conduits promote sciatic nerve regeneration

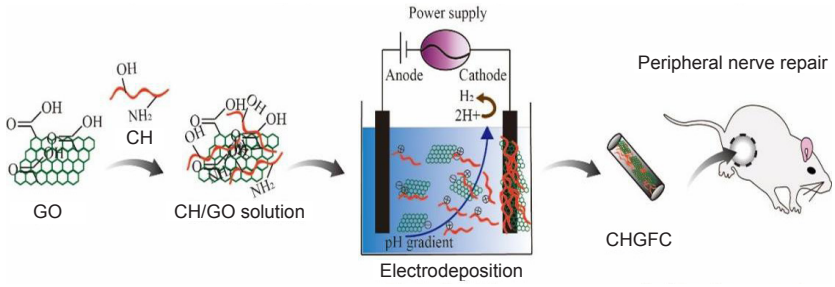

Abstract

Currently available commercial nerve guidance conduits have been applied in the repair of peripheral nerve defects. However, a conduit exhibiting good biocompatibility remains to be developed. In this work, a series of chitosan/graphene oxide (GO) films with concentrations of GO varying from 0–1 wt% (collectively referred to as CHGF-n) were prepared by an electrodeposition technique. The effects of CHGF-n on proliferation and adhesion abilities of Schwann cells were evaluated. The results showed that Schwann cells exhibited elongated spindle shapes and upregulated expression of nerve regeneration-related factors such as Krox20 (a key myelination factor), Zeb2 (essential for Schwann cell differentiation, myelination, and nerve repair), and transforming growth factor β (a cytokine with regenerative functions). In addition, a nerve guidance conduit with a GO content of 0.25% (CHGFC-0.25) was implanted to repair a 10-mm sciatic nerve defect in rats. The results indicated improvements in sciatic functional index, electrophysiology, and sciatic nerve and gastrocnemius muscle histology compared with the CHGFC-0 group, and similar outcomes to the autograft group. In conclusion, we provide a candidate method for the repair of peripheral nerve defects using free-standing chitosan/GO nerve conduits produced by electrodeposition.

Key Words: chitosan; electrodeposition; free-standing; graphene oxide; nerve conduit; nerve factors; Schwann cells; tissue engineerin

Introduction

Peripheral nerve injury (PNI) caused by trauma, burn, or surgical intervention is a global clinical problem that leads to complete or partial loss of motor, sensory, and autonomic functions, therefore drastically affecting the quality of life of patients (Mobini et al., 2019; Hussain et al., 2020; Chen et al., 2021; Zaminy et al., 2021). Regeneration following PNI is accompanied by a multiplex biological process in which Schwann cells (SCs) play an important role (Zaming et al., 2020a; Li et al., 2021). Mechanistically, SCs provide a suitable microenvironment for the inventory and regeneration of nerve cells, furnish vital nutrition, support cell adhesion, and guide directional nerve cell migration (Wang et al., 2021a, c; Cai et al., 2022). SCs inherently participate in Wallerian degeneration, whereby they contribute to phagocytosis of myelin and axon debris, axon regeneration, deposition of a supportive extracellular matrix, neurotrophin release, and macrophage recruitment to clear debris after PNI (Navarro et al., 2007; Novikova et al., 2008; Deumens et al., 2010; Carriel et al., 2017). Thus, implantation of a nerve guidance conduit (NGC) at the site of injury needs to support SC growth to benefit functional recovery of the injured nerve.

Artificial NGCs developed by tissue engineering from materials including polylactide-caprolactone, polylactic acid, chitosan (CH), collagen, graphene oxide (GO), and cellulose have been widely used for PNI repair (Siemionow et al., 2010; Wu et al., 2020). Among these components, CH is a cationic polysaccharide broadly applied in the field of peripheral nerve regeneration for its biocompatibility, biodegradability, and antimicrobial activity (Lau et al., 2018; Wu et al., 2021; Liu et al., 2022). The oxidized form of graphene, GO, has abundant oxygen-containing groups, such as hydroxyl (-OH) and carbonyl (-C=O) groups, a high specific surface area, good mechanical properties, flexibility, and excellent electrical conductivity (Reina et al., 2014; Gardin et al., 2016). In addition, GO is biocompatible at low concentrations (Nishida et al., 2014; Nagarajan et al., 2016) and acts as an alternative for reinforcing material (Han et al., 2011; Ouyang et al., 2015; Sayyar et al., 2015). Importantly, GO has also been shown to promote the proliferation of SCs, hippocampal cells, PC12 cells, and stem cells (Li et al., 2011b, 2016; Gardin et al., 2016; Liu et al., 2017),

CH-based NGCs can be prepared by chemical crosslinking or mold-forming techniques. The basic function of the NGC is to support the adhesion, proliferation, and migration of nerve and glial cells (Vijayavenkataraman, 2020). To improve the *in vivo* performance of CH-based NGCs, a series of material modification strategies were developed. Rao et al. (2020) designed an aligned-CH hydrogel NGC grafted with bioactive peptides, which yielded great application effects for repair of long-distance sciatic nerve defects. Chen et al. (2021) showed that depletion of interleukin 17F in the nerve regeneration microenvironment could improve the repair effect of CH-based NGCs. In addition, numerous physical and biological parameters were shown to be beneficial for nerve regeneration (Grinsell and Keating, 2014; Li et al., 2020). In this work, we hypothesized that incorporation of GO into CH-based NGCs could enhance their biocompatibility. No previous report has described a CH/GO composite NGC, likely because of a lack of an appropriate material processing technology.

[1]Department of Biomedical Engineering and Hubei Province Key Laboratory of Allergy and Immune Related Disease, School of Basic Medical Sciences, Wuhan University, Wuhan, Hubei Province, China; [2]Department of Interventional Radiology, The First Affiliated Hospital of Zhengzhou University, Zhengzhou, Henan Province, China; [3]Clinical Medical College, Hubei University of Science and Technology, Xianning, Hubei Province, China

*Correspondence to: Yong Zheng, PhD, zhengyong@whu.edu.cn; Yun Chen, PhD, yunchen@whu.edu.cn.

https://orcid.org/0000-0002-5872-9609 (Yong Zheng); https://orcid.org/0000-0002-5984-7455 (Yun Chen)

#These authors contributed equally.

Funding: *This study was supported by the National Natural Science Foundation of China, No. 81871493 (to YC) and the Medical Science Advancement Program (Clinical Medicine) of Wuhan University, No. TFLC2018003 (to YC).*

How to cite this article: *Zhao YN, Wu P, Zhao ZY, Chen FX, Xiao A, Yue ZY, Han XW, Zheng Y, Chen Y (2023) Electrodeposition of chitosan/graphene oxide conduit to enhance peripheral nerve regeneration. Neural Regen Res 18(1):207-212.*

Electrodeposition is an attractive material processing technique characterized by programmable assembly in response to device-imposed stimuli (Xi et al., 2009; Sun et al., 2015). Because of its self-assembling and pH-responsive properties, CH can be used to build a film on a conducting electrode using electrodeposition methods (Wang et al., 2005). Compared with conventional techniques, electrodeposition is a more facile and precise method to form stable CH films with controllable thickness, stiffness, and other properties on the electrode surface (Liu et al., 2014). Specifically, the oxygen-containing functional groups of GO greatly enhance its surface ability to bind other materials (Shen et al., 2012; Li et al., 2016). Thus, GO could be homogeneously dispersed into CH solution and subsequently co-deposited along with CH.

This work aimed to fabricate a series of CH/GO composite NGCs using a novel electrodeposition technique, and subsequently evaluate their chemical composition, surface morphology, and *in vitro* biocompatibility. Our findings suggest that the obtained CH/GO composite NGCs have relatively good performance *in vivo* for PNI repair.

Methods

Materials

Chitosan powder (200-kDa molecular weight and 80% deacetylation degree) was purchased from TCI Biotechnology (Shanghai, China). GO nanosheets were obtained from Hengqiu Technology (Suzhou, China). A spontaneously immortalized Schwann cell line RSC 96 (CSTR: 19375.09.3101RATGNR6; Serial: GNR 6) was supplied by the National Collection of Authenticated Cell Cultures (Shanghai, China). Fetal bovine serum, alpha minimum essential medium (α-MEM), trypsin/EDTA solution, and penicillin-streptomycin solution were supplied by Sigma (St. Louis, MO, USA). HCl, dimethyl sulfoxide (DMSO), and NaOH were provided by Sinopharm Chemical Reagent (Beijing, China). Other chemicals were used without further purification.

Electrodeposition of chitosan/graphene oxide composites

CH solution (CS, 1 wt%) was prepared by liquefying CH in a 0.25 M HCl solution under vigorous stirring, and then adjusting the pH value to 5.5 using 0.25 M NaOH solution. GO (0.2 wt%) was dispersed into deionized water under continuous stirring. The GO suspension was added to the CS solution and sonicated for 5 minutes to obtain a homogeneous solution. Next, the prepared CS/GO solution was transferred into a beaker for electrodeposition. A titanium plate (0.1 × 40 × 20 mm^3) served as the cathode and a platinum wire served as the anode. Electrodeposition was performed by immersing the titanium plate and 1.5 cm of the platinum wire into the CS/GO solution. A programmable DC power supply (Keithley, Shanghai, China) was employed to apply 5–6 V to these two electrodes for 1 hour, resulting in films with a thickness of ~3 mm. Following washing of films with distilled water to clear any unbound GO particles, they were dried for further studies. The resultant films were named CHGF-0/0.25/0.5/1 or collectively CHGF-n, where CH stands for chitosan, G for graphene oxide, F for film, and n for the concentration of GO (wt%) in the mixed solution. **Table 1** shows the sample names and compositions of various CHGF-n preparations. To further prepare CH/GO NGCs with GO contents of 0 and 0.25 wt%, we replaced the titanium plate of the cathode with a stainless-steel needle. The resultant conduits were named CHGFC-0 and CHGFC-0.25.

Table 1 | **Sample codes and compositions of films and conduits**

Sample code	CS (mL)	GO (mL)	Deionized water (mL)	Total volume (mL)	Sample type
CHGF-0	50	0	50	100	Film
CHGF-0.25	50	12.5	37.5	100	Film
CHGF-0.5	50	25	25	100	Film
CHGF-1	50	50	0	100	Film
CHGFC-0	50	0	50	100	Conduit
CHGFC-0.25	50	12.5	37.5	100	Conduit

CHGF: Chitosan/graphene oxide film; CHGFC: CHGF-based conduit; CS: chitosan; GO: graphene oxide.

Characterization of CHGF

Morphological analysis of CHGF was evaluated with a digital camera (Coolpix P6000, Nikon, Tokyo, Japan) and scanning electron microscope (SEM; TESCAN, Shanghai, China). For SEM analysis, gold was employed to sputter-coat the dried films, which were then observed with an accelerating voltage of 20 kV (Hu et al., 2019b, 2020). To evaluate sample cross-sections, samples were immersed in liquid nitrogen for 10 minutes, fractured, and then broken off to obtain a fresh section. A fourier transform infrared (FTIR) spectrometer (Nicolet, Waltham, MA, USA) was employed to record FTIR spectra in the wavelength range of 4000–500 cm^{-1}. Afterwards, an automated laser Raman microscope (Horiba, Villeneuve-d'Ascq, France) with an excitation wavelength of 633 nm was employed to characterize the chemical composition of CHGF. A WAXD diffractometer (Bruker, Waltham, MA, USA) in the 2θ range of 5°–40° with a 4°/min scan speed was employed to obtain X-ray powder diffraction (XRD) patterns.

The tensile strength of CHGF was determined with a universal testing machine (SANS, Dongguan, China) at 8 mm/min rate of elongation (Wang et al., 2020). CHGF samples were cut into 10 × 1 cm^2 pieces and immersed in phosphate-buffered saline (PBS) for 2 hours. Finally, careful blotting of the wet samples was performed with filter paper to remove the surface solution, and samples were immediately tested. Six samples were evaluated to determine the mean value.

Biocompatibility evaluations

3-[4,5-Dimethylthiazol-2-yl]-2,5 diphenyl tetrazolium bromide assay

The cytotoxicity of CHGF-n preparations was tested by 3-[4,5-dimethylthiazol-2-yl]-2,5-diphenyl tetrazolium bromide (MTT) assay. SCs were cultured with α-MEM containing 10% fetal bovine serum and 100 U/mL penicillin-streptomycin under 37°C and 5% CO_2 conditions. CHGF extracts were prepared by adding sterilized CHGF-n to α-MEM (0.2 g sample in 1 mL culture medium) and incubating at 37°C for 72 hours (Wang et al., 2021b).

SC viability and proliferation was detected using an MTT assay. Initially, cells were seeded in 96-well plates coated with laminin (2 × 10^3 cells/well) for incubation at 37°C for 24 hours. Next, extracts (50 μL) were added to the plate and cells were allowed to grow in 5% CO_2 at 37°C. Culture medium with cells but no extract was employed as a negative control, while culture medium without extract or cells was utilized as a blank control. Cells were allowed to grow for 24, 48, or 72 hours and then 20 μL of MTT solution (Beyotime, Suzhou, China) was mixed into wells and incubated for 4 hours at 37°C. Subsequently, 200 μL of DMSO was added. Swirling of the dissolved solution was performed for approximately 10 minutes with a shaker to obtain a homogenous solution. The absorbance of each well was measured with a microplate reader (Shimadzu UV-1601, Shanghai, China) at a 490-nm wavelength. The following formula was employed to compute cell viability:

$$\text{Cell viability (\%)} = (A_S - A_B) / (A_N - A_B) \times 100$$

In which A_S, A_N, and A_B denote the absorption values of the sample, negative control, and blank control, respectively.

Cell contact experiments

To explore the potential utilization of CHGF as an NGC, SCs were directly cultured on the samples to observe their behaviors. Prior to the seeding stage, CHGF was sterilized and washed three times with distilled water. For cell morphology observation, SCs were seeded at a density of 5 × 10^4 cells per well on the surface of CHGF and incubated for 72 hours in 5% CO_2 at 37°C. Tissue culture plastic coated with laminin was used as a control. After incubation, cells on the films were fixed with 3.7% paraformaldehyde solution overnight at room temperature. The following day, fixed cells on the surfaces of CHGF samples were dehydrated in a graded series of ethanol solutions (Zhao et al., 2018b). Finally, samples were coated with gold under vacuum for observation by SEM. SCs on the surface of CHGF were further identified by calcein acetoxymethyl ester (calcein AM) staining (50 μg; Calcein AM Assay Kit, ab141420; Abcam, Cambridge, UK). Briefly, SCs on samples were stained with AM dye for 30 minutes at 37°C. Finally, samples were rinsed three times with PBS and observed by fluorescence microscopy (Olympus, Tokyo, Japan).

Quantitative reverse transcription-polymerase chain reaction analysis

mRNA expression of *Krox20* (a key myelination factor), transforming growth factor β (*TGF-β*, a cytokine with regenerative functions), and *Zeb2* (essential for Schwann cell differentiation, myelination, and nerve repair) was evaluated in SCs cultured with CHGF-n extracts. After SCs were planted onto tissue culture plastic or CHGF for 72 hours, mRNA expression levels of *Krox20*, *Zeb2*, and *TGF-β* in SCs were determined with quantitative reverse transcription-polymerase chain reaction (qRT-PCR). First, total cellular RNA was extracted from SCs with TRIzol™ reagent (Sigma) according to the manufacturer's instructions. Next, cDNA was transcribed from total cellular RNA with a cDNA Synthesis Kit (Thermo Fisher Scientific, Waltham, MA, USA). Next, Maxima SYBR Green or ROX qPCR Master Mix was employed to perform qRT-PCR. The temperature gradient of amplification was as follows: 95°C for 15 minutes; and 40 cycles of 15 seconds at 94°C, 30 seconds at 60°C, and 30 seconds at 72°C. Relative expression levels were calculated using the comparative $2^{-\Delta\Delta Ct}$ method. Primers used in this study are listed in **Table 2**.

Table 2 | **Primer sequences for quantitative reverse transcription-polymerase chain reaction**

Gene	Primer sequence (5'–3')	Product size (bp)
Krox20	F: CGA GGA GCA AAT GAT GAC CG	89
	R: ATC ATG CCA TCT CCA GCC ACT	
Zeb2	F: AAA GCA GTT CCC TTC TGC GA	102
	R: AGG AGC CCG AGT GTG AAA AG	
TGF-β	F: CTG CTG ACC CCC ACT GAT AC	97
	R: AGC CCT GTA TTC CGT CTC CT	
GAPDH	F: AGT GCC AGC CTC GTC TCA TA	122
	R: GGT AAC CAG GCG TCC GAT AC	

F: Forward; GAPDH: glyceraldehyde 3-phosphate dehydrogenase; R: reverse; TGF-β: transforming growth factor β.

Animals and surgical procedures
All animal experiments were performed in accordance with Guiding Opinions on the Treatment of Laboratory Animals issued by the Ministry of Science and Technology of the People's Republic of China, and approved by the Animal Care and Welfare Committee of the Wuhan University School of Medicine (2018116) on October 22, 2018. Forty-two female Sprague-Dawley rats (200–220 g) were provided by Wuhan University Laboratory Animal Center (Wuhan, Hubei Province, China), and then randomly divided into three groups: autograft, CHGFC-0, and CHGFC-0.25. For surgical procedures, animals were anesthetized by an intraperitoneal administration of 1% pentobarbital sodium (150 mg/kg) (Sigma). Next, the sciatic nerve in the right hind limb was exposed and a 10-mm nerve defect was created and repaired with autograft or a CHGFC conduit. For the autograft group, the excised autograft was rotated by 180° and sutured to the proximal and distal nerve stumps. In CHGFC-0 and CHGFC-0.25 groups, conduits with GO contents of 0% and 0.25% were sutured to the proximal and distal nerve stumps of the injured nerve. After transplantation, the musculature and skin were sutured. All procedures were performed under aseptic conditions and penicillin (3 mg/kg) was administered postoperatively for 3 days. After 90 days, rats were euthanized and evaluated for nerve regeneration.

Sciatic functional index
To explore functional recovery after surgery, sciatic functional index (SFI) was evaluated at 90 days. Black ink was applied to the hind paws of rats, which were subsequently placed in a 15 × 100 cm corridor covered with a sheet of white paper. Three parameters including print length (PL: longest distance from toe to heel), intermediate toe spread (IT: distance from the second to fourth toes), and toe spread (TS: distance from first to fifth toes) were obtained from the paw prints. Data for normal (N) and experimental (E) hind legs were utilized. The formula SFI = (–38.3 × (EPL – NPL)/NPL) + (13.3 × (EIT – NIT)/NIT) + (109.5 × (ETS – NTS)/NTS) – 8.8 was employed to compute SFI. SFI values range between –100 and 0, with –100 denoting complete dysfunction of nerves and 0 denoting good function.

Electrophysiological test
Electrophysiological studies were also used to evaluate functional recovery of the regenerated nerve. At 90 days after implantation, rats were anesthetized and the sciatic nerve on the operative side was re-exposed. A stimulation electrode was applied to the proximal nerve trunk of the rat, and compound muscle action potentials (CMAPs) of the gastrocnemius belly on the operative side were recorded. The stimulating mode was set to pulse mode with a 1-Hz frequency, 10-mV stimulus intensity, and 1-ms duration.

Histological detection of nerve regeneration
At 90 days after implantation, the distal nerve ends of each group were obtained and fixed in 2.5% glutaraldehyde overnight. After washing with PBS, samples were post-fixed in 1% osmium tetraoxide (Sigma) for 1 hour, cleaned, dehydrated, and embedded in Epon 812 epoxy resin (Sigma). Next, the epoxy resin was cut into ultrathin sections of 50 nm thickness and stained with lead citrate and uranyl acetate. Finally, stained sections were examined by transmission electron microscopy (FEI, Thermo Fisher Scientific). Image-Pro Plus 6.0 (Media Cybernetics, Silver Spring, MD, USA) was employed to obtain the area of myelinated axons, thickness of myelin sheaths, and number of myelin sheaths.

Gastrocnemius muscle measurement and histological assessment
Morphology and function of the gastrocnemius muscle are reliable parameters to examine nerve regeneration (Xue et al., 2017). At 90 days after implantation, the bilateral gastrocnemius muscles were dissected and weighed. The muscle recovery ratio was calculated as the right-side weight divided by the left-side weight. Next, gastrocnemius muscles were stored in 4% paraformaldehyde until staining with a Masson's Trichrome Staining Kit (Beyotime) to visualize collagen contents. Images of five randomly selected fields in each sample were acquired with a light microscope (Olympus). Image-Pro Plus software was employed to determine the cross-sectional areas of muscle and collagen fibers. The percentage area of collagen fibers was calculated as the collagen fiber area divided by the sum of collagen and muscle fiber areas.

Statistical analysis
No blinded method was applied in the collection or analysis of the results. Data are expressed as the mean ± standard deviation. Statistical comparisons were performed by one-way analysis of variance (ANOVA) followed by the least significant difference test using SPSS 20.0 (IBM, Armonk, NY, USA). $P < 0.05$ was considered statistically significant.

Results

Fabrication of CHGF
The increased pH gradient generated close to the electrode causes CH electrodeposition on the cathode (Zhao et al., 2014). GO sheets are chemically reduced in aqueous solutions, leading to their irreversible agglomeration (Stankovich et al., 2007). Thus, it is reasonable to speculate that the GO sheets could directly attach to the electrode surface (Chen et al., 2011). When a voltage is applied, protons around the electrode surface are consumed, leading to a relatively high localized pH. As a result, the positively charged CS chains and negatively charged GO wrap around to the cathode and are co-deposited from bulk solution together. Conclusively, the electrodeposition method is a simple and alternative strategy to fabricate CHGF on conductive substrates.

Characterization of CHGF
Optical images of CHGF-n are shown in **Figure 1A**. It was observed that CHGF-0 was transparent, while CHGF-0.25, CHGF-0.5, and CHGF-1 appeared light brown, dark brown, and black, respectively. These results confirmed that GO was successfully electrodeposited together with CH. Next, the microstructure of CHGF-n was observed by SEM. As shown in **Figure 1B**, CHGF-0 exhibited a rough surface morphology. Compared with CHGF-0, CHGF-0.25 exhibited the typical crumpled and wrinkled texture associated with the presence of flexible and ultrathin graphene flakes (Liu et al., 2013). These flakes were evenly distributed among the film surface, providing physical cues for cell adhesion growth. In addition, several studies documented that GO could be used as chemical cue to enhance nerve cell growth and neurite extension (Liu et al., 2017). However, the surface changed as the GO content increased, with CHGF-0.5 exhibiting flake-like structures and CHGF-1 exhibiting a relatively smooth surface, potentially caused by GO accumulation. **Figure 1C** displays SEM images of CHGF-n cross-sections. The cross-section structure of CHGF-0 was observed to be smooth. When the addition of GO, uniform flake-like structures appeared on the cross-section of CHGF-0.25. This flake-like structure was replace by a more obvious multilayered structure in CHGF-0.5. However, the multilayered structure appeared slightly deteriorated in CHGF-1, likely owing to the excessive GO added to CS during the electrodeposition process. Conclusively, GO could be evenly dispersed within the CH film and the structure of deposited CHGF-n was influenced by the proportion of GO.

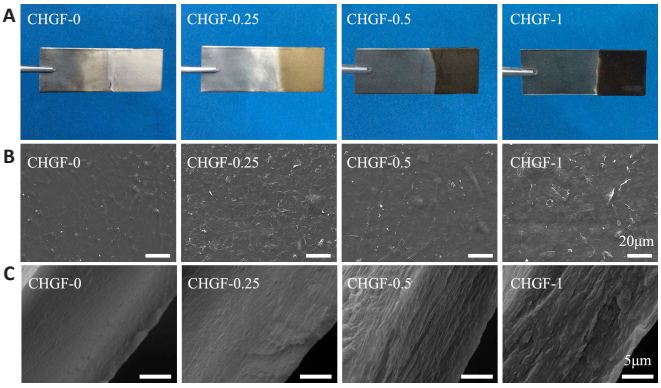

Figure 1 | Morphological observations of prepared CHGF composite nerve conduits.
Optical images (A) and scanning electron microscope images of the surfaces (B) and cross-sections (C) of CHGF-n [where n = graphene oxide of 0, 0.25, 0.5 and 1 (wt%) in the mixed solution]. CHGF: Chitosan/graphene oxide film.

Figure 2A displays the FTIR spectra of CH, GO, and CHGF-n preparations. Bands at 3368, 1735, 1621, 1398, and 1051 cm^{-1} of GO were attributed to the stretching vibrations of hydroxyl groups, stretching vibrations of carboxylic acid, skeletal vibrations of unoxidized graphitic domains, O-H deformations of the C-OH groups, and C=O stretching vibrations, respectively (Zhang et al., 2017). The FTIR spectrum of CH showed bands at 1655 cm^{-1} and 1581 cm^{-1} that were assigned to amide I and amide II, respectively. CHGF-n exhibited characteristic bands of CH at about 1655 and 1581 cm^{-1}, verifying the presence of CH in CHGF-n. However, characteristic bands of GO were not observed in the FTIR spectra of CHGF-0.25, CHGF-0.5, or CHGF-1 because the amount of GO was too small. Thus, Raman spectra were further employed to confirm GO incorporation. The Raman spectra of CHGF-n preparations are shown in **Figure 2C**. CHGF-0.25, CHGF-0.5, and CHGF-1 exhibited an obvious diamondoid band at 1290 cm^{-1} and graphitic band at 1600 cm^{-1} that were attributed to the two vibration modes of graphene (Ferrari, 2007). In contrast, CHGF-0 did not exhibit diamondoid or graphitic bands. **Figure 2B** indicates the XRD pattern of CHGF. In the XRD profile of GO, the strong diffraction peak at 11.2° was linked to the presence of oxygen-abundant groups on both sides of the nanosheets, along with the water molecules trapped between nanosheets (Rajabzadeh et al., 2014). CH displayed two sharp peaks at 9.8° and 19.9°, consistent with previous reports. Peaks of CHGF-n observed at 9°–11° and 19°–20° were slightly weaker compared with those of GO and CS, indicating a minor decrease in crystallinity. Collectively, these results indicate that the resultant CHGF was fabricated on the electrode by a green and precise electrodeposition method.

Figure 2D displays the tensile strength of CHGF-n preparations. Compared with CHGF-0, the film tensile strength increased with GO concentration to reach 0.58 ± 0.25 MPa for CHGF-0.5. This demonstrates that GO addition could enhance the mechanical properties of CHGF, consistent with previous research (Shen et al., 2012). Nevertheless, incremental increases in GO contents of the film reduced its tensile strength, probably because of deterioration of the multilayered structure, as indicated in **Figure 1C**. These results illustrate that the addition of GO enhanced the mechanical properties of neat CHGF-0, resulting in the peeling off of films from the titanium plate as a free-standing chitosan/graphene oxide matrix to construct CHGFC.

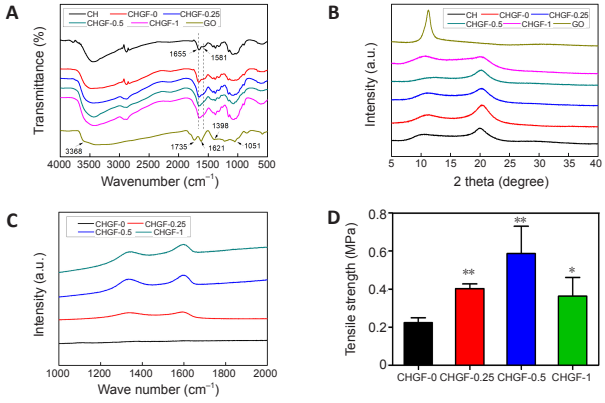

Figure 2 | Physicochemical properties of chitosan/GO composite nerve conduits.
Fourier transform infrared spectroscopy (FTIR) spectra (A), X-ray diffraction spectra (B) and Raman spectra (C) of raw materials (chitosan and graphene oxide) and CHGF-n [where *n* = graphene oxide of 0, 0.25, 0.5 and 1 (wt%) in the mixed solution]. The tensile strength (D) of CHGF-n in a wet condition, *n* = 3. **P* < 0.05, ***P* < 0.01, *vs*. CHGF-0 group. One-way analysis of variance followed by the least significant difference test was used for statistical analysis. At least three independent experiments were performed. CHGF: Chitosan (CH)/graphene oxide (GO) film.

Effects of CHGF on SC growth and behaviors *in vitro*

As shown in **Figure 3A**, the activity of SCs on CHGF-0.25 was highest at 24 hours, but decreased on CHGF-0.5 and CHGF-1, consistent with the notion that GO has dose-cytotoxicity. At 48 hours, the cell activity of each group was higher compared with that at 24 hours, and cell activity on CHGF-0.25 remained the highest. At 72 hours, cell activities on CHGF-0, CHGF-0.5, and CHGF-1 began to decrease. However, CHGF-0.25 retained a remarkable increase of cell viability compared with the control group. These results clearly suggest that cell viability depended on GO content and cell culture duration, and the excellent cytocompatibility of CHGF-0.25 makes it a promising material to construct CHGFC for peripheral tissue engineering applications.

Figure 3C shows SEM images of SCs on CHGF-n. Cells cultured on the CHGF-0, CHGF-0.5, and CHGF-1 were round and clustered together, which may be caused by the hydrophobic surface, microstructure, and chemical composition of these three samples. Cells cultured on CHGF-0.25 were well spread out and exhibited long spindle shapes, possibly due to its hydrophilic characteristics. SCs were further characterized by immunofluorescence staining. As shown in **Figure 3B**, in contrast to cells on other samples, cells cultured on CHGF-0.25 had spindle shapes. Therefore, samples with a GO content of 0.25% were identified as the favorable cell carrier to promote the spread and growth of SCs.

As shown in **Figure 3D–F**, mRNA expression levels of *Krox20*, *TGF-β*, and *Zeb2* in all CHGF-n groups were remarkably higher compared with the control group. Additionally, mRNA expression levels were relatively increased in the CHGF-0.25 group. Conclusively, CHGF-n, especially CHGF-0.25, promoted expression of nerve-related factors such as Krox20, Zeb2 and TGF-β, thus ensuring the regeneration of damaged nerves. Collectively, the results described above show that CHGF-0.25 had the most suitable surface structure, mechanical properties, and cell compatibility for SC growth, and the best performance for nerve-related factor secretion. Thus, the conduit referred to as CHGFC-0.25 (based on CHGF-0.25) was selected for animal experiments to evaluate nerve repair effects. CHGFC-0 and autograft groups were used as controls.

Animal experiments for CHGFC

Motor function of rats

There was a remarkable improvement in motor function of the CHGFC-0.25 group compared with the CHGFC-0 group (**Figure 4A**). SFI values of the CHGFC-0.25 group were similar to those of the autograft group, but SFI values of the CHGFC-0 group were significantly lower compared with autograft and CHGFC-0.25 groups ($P < 0.01$ and $P < 0.05$, respectively; **Figure 4B**). CMAP amplitudes on the surgical side of the CHGFC-0 and CHGFC-0.25 groups were significantly lower compared with the autograft group ($P < 0.01$ and $P < 0.05$, respectively; **Figure 4D**).

Morphology of regenerated nerves

As shown in **Figure 5A**, regenerated myelinated fibers were scattered in clusters (with the exception of an occasional unmyelinated fiber) and myelinated axons were coated with a clear myelin sheath in the autograft group. Structures of myelinated fibers in the CHGFC-0.25 group were similar to those of the autograft group. In contrast, myelinated fibers were seldom observed in the CHGFC-0 group. Areas of myelinated axons, thicknesses of myelin sheaths, and numbers of myelin sheath layers were significantly decreased in the CHGFC-0 group compared with the autograft group ($P < 0.05$ or $P < 0.01$; **Figure 5B–D**), while thicknesses of myelin sheaths and numbers of myelin sheath layers were significantly increased the CHGFC-25 group compared with the CHGFC-0 group ($P < 0.01$ and $P < 0.05$). Regenerated nerves in the CHGFC-0.25 group showed better recovery compared with the CHGFC-0 group but remained inferior to the autograft group.

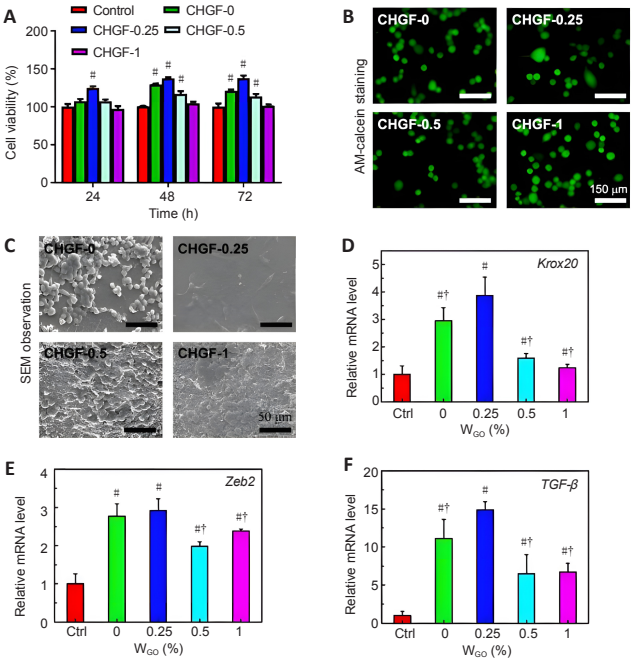

Figure 3 | CH/GO composite nerve conduits exhibited excellent biocompatibility towards SCs *in vitro*.
Cell viability of SCs co-incubated with extracts from CHGF-n [where n = graphene oxide content of 0, 0.25, 0.5 and 1 (wt%) in the mixed solution] for 24, 48, and 72 hours (A), *n* = 6. Calcein AM (calcein acetoxymethyl ester) staining (B) and SEM (C) images of SCs grown on the surface of CHGF-n for 72 hours. Scale bars: 150 μm in B, 50 μm in C. (D–F) *Krox20* (D), *Zeb2* (E), and *TGF-β* (F) expression of SCs cultured with extracts from CHGF-n for 72 hours as determined by quantitative reverse transcription polymerase chain reaction, *n* = 3. Green represents living cells. #*P* < 0.05, *vs*. control group; †*P* < 0.05, *vs*. CHGF-0.25 group (one-way analysis of variance followed by the least significant difference test). Untreated cells were used for the control group. WGO (%) represents the amount of GO. At least three independent experiments were performed. CHGF: Chitosan (CH)/graphene oxide (GO) film; SC: Schwann cell; SEM: scanning electron microscopy; TGF-β: transforming growth factor β.

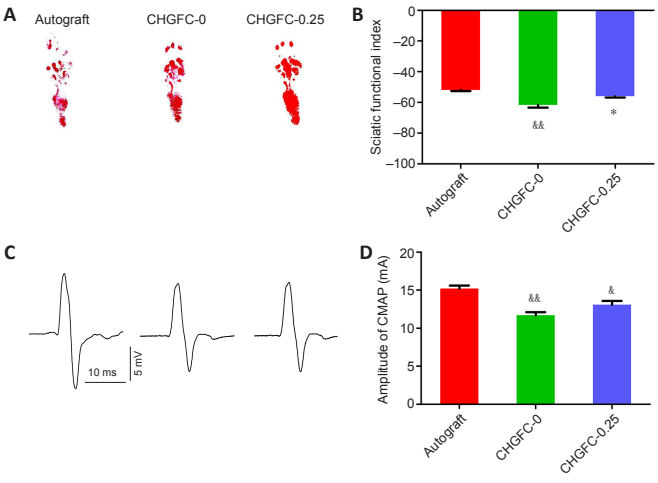

Figure 4 | CHGFC-0.25 improved the motor function of rats with peripheral nerve injury 90 days after transplantation.
(A) Representative footprint of the operative paw of rats. (B) Histograms showing the sciatic functional index detected on the injured side, *n* = 3. (C) Representative CMAP recordings of autograft (left), CHGFC-0 (middle), and CHGFC-0.25 (right) groups. (D) Histograms showing CMAP amplitudes detected on the injured side, *n* = 3. &*P* < 0.05, &&*P* < 0.01, *vs*. autograft group; **P* < 0.05, *vs*. CHGFC-0 group. One-way analysis of variance followed by the least significant difference test was used for statistical analysis. Three independent experiments were performed. CHGFC-0 and CHGFC-0.25: nerve guidance conduits with GO contents of 0% and 0.25%, respectively. CHGF: Chitosan/graphene oxide film; CHGFC: CHGF-based conduit; CMAP: compound muscle action potential; GO: graphene oxide.

Morphology and function of target muscles

As displayed in **Figure 6A** and **B**, gastrocnemius muscle dystrophy on the operative side of the CHGFC-0 group was more obvious compared with that of the autograft group. Results shown in **Figure 6C–E** indicate that muscle recovery of the CHGFC-0 group was worse compared with the autograft group, while muscle recovery of the CHGFC-0.25 group was similar to that of the autograft group.

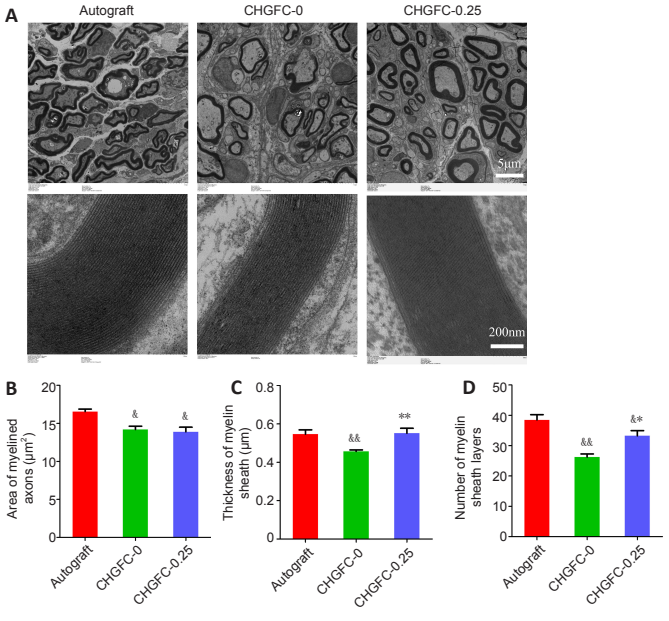

Figure 5 | **Histology of sciatic nerve 90 days after transplantation.**
Representative transmission electron micrographs of regenerated nerve on the operative side of autografts in CHGFC-0 and CHGFC-0.25 groups (A). Scale bars: 5 μm (upper) and 200 nm (lower). Histograms showing the area of myelinated axons (B, $n = 3$), thickness of myelin sheath (C, $n = 6$), and number of myelin sheath layers (D, $n = 4$). &$P < 0.05$, &&$P < 0.01$, *vs.* autograft group; *$P < 0.05$, **$P < 0.01$, *vs.* CHGFC-0 group (one-way analysis of variance followed by the least significant difference test). Three independent experiments were performed. CHGFC-0 and CHGFC-0.25: Nerve guidance conduits with GO contents of 0 and 0.25%, respectively. CHGF: Chitosan/graphene oxide film; CHGFC: CHGF-based conduit; GO: graphene oxide.

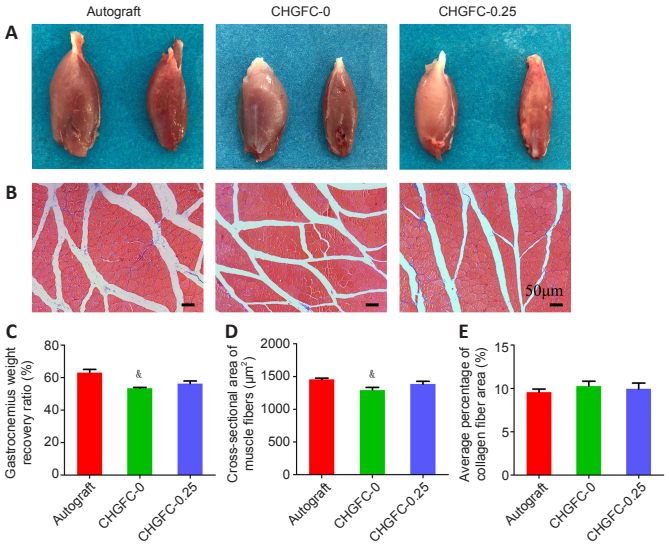

Figure 6 | **CHGFC-0.25 promoted gastrocnemius muscle regeneration.**
(A) Representative images of gastrocnemius muscle on normal and operative sides of autografts in CHGFC-0 and CHGFC-0.25 groups, respectively. (B) Masson's trichrome staining images of sectioned gastrocnemius muscle on the operative side of autografts in CHGFC-0 and CHGFC-0.25 groups, respectively. Scale bars: 50 μm. Red parts represent muscle fibers and blue parts represent collagen fibers. (C, D) Statistical analysis of the gastrocnemius weight recovery ratio (C, $n = 3$), cross-sectional area of muscle fibers (D, $n = 4$), and average percentage of collagen fiber area (E, $n = 3$) for each group. &$P < 0.05$, *vs.* autograft group (one-way analysis of variance followed by the least significant difference test). Three independent experiments were performed. CHGFC-0 and CHGFC-0.25: nerve guidance conduits with GO contents of 0% and 0.25%, respectively. CHGF: Chitosan/graphene oxide film; CHGFC: CHGF-based conduit; GO: graphene oxide.

Discussion

CH is an ideal biomedical polymer that can be processed by mold-forming and other techniques (Hu et al., 2019a). In our previous works, we successfully developed a variety of CH-based NGCs. On this basis, the *in vivo* application effect of these CH-based NGCs was further improved by physicochemical and biological methods. For example, multi-channel NGCs were prepared to promote the proliferation and directional migration of nerves cells, effectively shortening the time required for nerve recanalization (Zhao et al., 2018a). Electrodeposition, a simple and efficient material processing technology, has been widely used for surface modification of metal devices. Our group and cooperative teams successfully introduced electrodeposition technology into the field of biomaterials, and successively developed a series of chitin/CH biomaterials with good economic benefits (Zhao et al., 2018a; Liu et al., 2021).

Preliminary progress has been made in the development of electrodeposited CH-based NGCs. Notably, this work revealed for the first time that GO could effectively improve the biocompatibility and bioactivity of CH-based NGCs for glial cells, and thus improve the application effect *in vivo*. GO is an inorganic non-metallic material with desirable conductivity and biodegradability. Owning to its high performance, publications describing GO in the field of biomedical materials have consistently increased annually (Shende and Pathan, 2021). Our results showed that the introduction of GO into CH significantly changed the chemical composition, micro-structure, mechanical strength, and biocompatibility of the obtained composite NGC. Thus, inclusion of GO might be a key reason for the promotive effects observed for NGCs. In recent years, the biological mechanism of GO has been revealed. We assumed that GO could be swallowed by glial cells during degradation *in vivo*, whereby it participates in intracellular signal transduction to synergistically promote nerve regeneration. In conclusion, a GO-modified CH-based NGC prepared by electrodeposition technique promoted the treatment effect for PNI, which was attributed to synergistic effects between the NGC and glial cells. Above all, the application of GO can be refined into a general strategy to upgrade existing NGC materials.

Limitations

Even animals with permanently sectioned sciatic nerves tend to develop locomotor strategies that partially compensate for the loss in function induced by nerve damage. Thus, an additional experimental group with impeded reinnervation (a negative control group) is necessary to evaluate the magnitude of treatment responses.

Conclusions

In this study, we constructed a series of CHGFs and evaluated their physicochemical and biological properties. *In vitro* experiments showed that GO was successfully inserted in CHGF to enhance its mechanical properties, thus promoting CHGF to peel off from the mold to form free-standing films. CHGF-0.25 significantly enhanced SC growth, extension, and secretion of nerve-related factors such as Krox20, Zeb2, and TGF-β. *In vivo* results showed that CHGFC-0.25 could guide the regeneration of injured nerves, thus representing a candidate strategy for peripheral nerve repair. CHGFC prepared by electrodeposition is green, simple, accurate, nontoxic, and harmless, and provides a new direction for preparation of NGCs.

Acknowledgments: *The authors are grateful to the Experimental Teaching Center of Basic Medical Sciences, Wuhan University for technical support.*
Author contributions: *YNZ, PW and YC designed the study and drafted the manuscript. ZYZ, FXC and AX conducted surgery and behavioral tests. ZYY and YZ carried out histology and image analysis. XWH and YZ helped to draft the manuscript. YC performed manuscript editing and review. All authors read and approved the final manuscript for publication.*
Conflicts of interest: *The all authors declare no competing financial interest.*

References

Cai M, Shao J, Yung B, Wang Y, Gao NN, Xu X, Zhang HH, Feng YM, Yao DB (2022) Baculoviral inhibitor of apoptosis protein repeat-containing protein 3 delays early Wallerian degeneration after sciatic nerve injury. Neural Regen Res 17:845-853.

Carriel V, Garzon I, Campos A, Cornelissen M, Alaminos M (2017) Differential expression of GAP-43 and neurofilament during peripheral nerve regeneration through bio-artificial conduits. J Tissue Eng Regen Med 11:553-563.

Chen F, Liu W, Zhang Q, Wu P, Xiao A, Zhao Y, Zhou Y, Wang Q, Chen Y, Tong Z (2021) IL-17F depletion accelerates chitosan conduit guided peripheral nerve regeneration. Acta Neuropathol Commun 9:125.

Chen L, Tang Y, Wang K, Liu C, Luo S (2011) Direct electrodeposition of reduced graphene oxide on glassy carbon electrode and its electrochemical application. Electrochem Commun 13:133-137.

Deumens R, Bozkurt A, Meek MF, Marcus MA, Joosten EA, Weis J, Brook GA (2010) Repairing injured peripheral nerves: Bridging the gap. Prog Neurobiol 92:245-276.

Ferrari AC (2007) Raman spectroscopy of graphene and graphite: Disorder, electron-phonon coupling, doping and nonadiabatic effects. Solid State Commun 143:47-57.

Gardin C, Piattelli A, Zavan B (2016) Graphene in regenerative medicine: focus on stem cells and neuronal differentiation. Trends Biotechnol 34:435-437.

Grinsell D, Keating CP (2014) Peripheral nerve reconstruction after injury: a review of clinical and experimental therapies. Biomed Res Int 2014:698256.

Han D, Yan L, Chen W, Li W (2011) Preparation of chitosan/graphene oxide composite film with enhanced mechanical strength in the wet state. Carbohydr Polym 83:653-658.

Hu W, Wang Z, Xiao Y, Zhang S, Wang J (2019a) Advances in crosslinking strategies of biomedical hydrogels. Biomater Sci 7:843-855.

Hu W, Wang Z, Xu Y, Wang X, Xiao Y, Zhang S, Wang J (2019b) Remodeling of inherent antimicrobial nanofiber dressings with melamine-modified fibroin into neoskin. J Mater Chem B 7:3412-3423.

Hu W, Wang Z, Zha Y, Gu X, You W, Xiao Y, Wang X, Zhang S, Wang J (2020) High flexible and broad antibacterial nanodressing induces complete skin repair with angiogenic and follicle regeneration. Adv Healthc Mater 9:2000035.

Hussain G, Wang J, Rasul A, Anwar H, Qasim M, Zafar S, Aziz N, Razzaq A, Hussain R, de Aguilar JG, Sun T (2020) Current status of therapeutic approaches against peripheral nerve injuries: a detailed story from injury to recovery. Int J Biol Sci 16:116-134.

Lau YT, Kwok LF, Tam KW, Chan YS, Shum DK, Shea GK (2018) Genipin-treated chitosan nanofibers as a novel scaffold for nerve guidance channel design. Colloids Surf B Biointerfaces 162:126-134.

Li G, Zhao Y, Zhang L, Gao M, Kong Y, Yang Y (2016) Preparation of graphene oxide/polyacrylamide composite hydrogel and its effect on Schwann cells attachment and proliferation. Colloids Surf B Biointerfaces 143:547-556.

Li L, Xu Y, Wang X, Liu J, Hu X, Tan D, Li Z, Guo J (2021) Ascorbic acid accelerates Wallerian degeneration after peripheral nerve injury. Neural Regen Res 16:1078-1085.

Li N, Zhang X, Song Q, Su R, Zhang Q, Kong T, Liu L, Jin G, Tang M, Cheng G (2011) The promotion of neurite sprouting and outgrowth of mouse hippocampal cells in culture by graphene substrates. Biomaterials 32:9374-9382.

Li R, Li DH, Zhang HY, Wang J, Li XK, Xiao J (2020) Growth factors-based therapeutic strategies and their underlying signaling mechanisms for peripheral nerve regeneration. Acta Pharmacol Sin 41:1289-1300.

Liu FD, Duan HM, Hao F, Zhao W, Gao YD, Hao P, Yang ZY, Li XG (2022) Biomimetic chitosan scaffolds with long-term controlled release of nerve growth factor repairs 20-mm-long sciatic nerve defects in rats. Neural Regen Res 17:1146-1155.

Liu H, Zhao Y, Tong J, Shi X, Chen Y, Du Y (2021) Electrofabrication of flexible and mechanically strong tubular chitosan implants for peripheral nerve regeneration. J Mater Chem B 9:5537-5546.

Liu J, Wang X, Wang T, Li D, Xi F, Wang J, Wang E (2014) Functionalization of monolithic and porous three-dimensional graphene by one-step chitosan electrodeposition for enzymatic biosensor. ACS Appl Mater Interfaces 6:19997-20002.

Liu X, Miller AL, 2nd, Park S, Waletzki BE, Zhou Z, Terzic A, Lu L (2017) Functionalized carbon nanotube and graphene oxide embedded electrically conductive hydrogel synergistically stimulates nerve cell differentiation. ACS Appl Mater Interfaces 9:14677-14690.

Liu Y, Yang S, Niu W (2013) Simple, rapid and green one-step strategy to synthesis of graphene/carbon nanotubes/chitosan hybrid as solid-phase extraction for square-wave voltammetric detection of methyl parathion. Colloids Surf B Biointerfaces 108:266-270.

Mobini S, Song YH, McCrary MW, Schmidt CE (2019) Advances in ex vivo models and lab-on-a-chip devices for neural tissue engineering. Biomaterials 198:146-166.

Nagarajan S, Pochat-Bohatier C, Teyssier C, Balme S, Miele P, Kalkura N, Cavaillès V, Bechelany M (2016) Design of graphene oxide/gelatin electrospun nanocomposite fibers for tissue engineering applications. RSC Advances 6:109150-109156.

Navarro X, Vivo M, Valero-Cabre A (2007) Neural plasticity after peripheral nerve injury and regeneration. Prog Neurobiol 82:163-201.

Nishida E, Miyaji H, Takita H, Kanayama I, Tsuji M, Akasaka T, Sugaya T, Sakagami R, Kawanami M (2014) Graphene oxide coating facilitates the bioactivity of scaffold material for tissue engineering. Jpn J Appl Phys 53:06JD04.

Novikova LN, Pettersson J, Brohlin M, Wiberg M, Novikov LN (2008) Biodegradable poly-beta-hydroxybutyrate scaffold seeded with Schwann cells to promote spinal cord repair. Biomaterials 29:1198-1206.

Ouyang A, Wang C, Wu S, Shi E, Zhao W, Cao A, Wu D (2015) Highly porous core-shell structured graphene-chitosan beads. ACS Appl Mater Interfaces 7:14439-14445.

Rajabzadeh S, Rounaghi GH, Arbab-Zavar MH, Ashraf N (2014) Development of a dimethyl disulfide electrochemical sensor based on electrodeposited reduced graphene oxide-chitosan modified glassy carbon electrode. Electrochim Acta 135:543-549.

Rao F, Wang Y, Zhang D, Lu C, Cao Z, Sui J, Wu M, Zhang Y, Pi W, Wang B, Kou Y, Wang X, Zhang P, Jiang B (2020) Aligned chitosan nanofiber hydrogel grafted with peptides mimicking bioactive brain-derived neurotrophic factor and vascular endothelial growth factor repair long-distance sciatic nerve defects in rats. Theranostics 10:1590-1603.

Reina G, Tamburri E, Orlanducci S, Gay S, Matassa R, Guglielmotti V, Lavecchia T, Terranova ML, Rossi M (2014) Nanocarbon surfaces for biomedicine. Biomatter 4:e28537.

Sayyar S, Murray E, Thompson BC, Chung J, Officer DL, Gambhir S, Spinks GM, Wallace GG (2015) Processable conducting graphene/chitosan hydrogels for tissue engineering. J Mater Chem B 3:481-490.

Shen J, Yan B, Li T, Long Y, Li N, Ye M (2012) Study on graphene-oxide-based polyacrylamide composite hydrogels. Compos Part A Appl Sci Manuf 43:1476-1481.

Shende P, Pathan N (2021) Potential of carbohydrate-conjugated graphene assemblies in biomedical applications. Carbohydr Polym 255:117385.

Siemionow M, Bozkurt M, Zor F (2010) Regeneration and repair of peripheral nerves with different biomaterials: review. Microsurgery 30:574-588.

Stankovich S, Dikin DA, Piner RD, Kohlhaas KA, Kleinhammes A, Jia Y, Wu Y, Nguyen ST, Ruoff RS (2007) Synthesis of graphene-based nanosheets via chemical reduction of exfoliated graphite oxide. Carbon 45:1558-1565.

Sun W, Wang X, Lu Y, Gong S, Qi X, Lei B, Sun Z, Li G (2015) Electrochemical deoxyribonucleic acid biosensor based on electrodeposited graphene and nickel oxide nanoparticle modified electrode for the detection of salmonella enteritidis gene sequence. Mater Sci Eng C Mater Biol Appl 49:34-39.

Vijayavenkataraman S (2020) Nerve guide conduits for peripheral nerve injury repair: A review on design, materials and fabrication methods. Acta Biomater 106:54-69.

Wang XQ, Duan XM, Liu LH, Fang YQ, Tan Y (2005) Carboxyfluorescein diacetate succinimidyl ester fluorescent dye for cell labeling. Acta Biochim Biophys Sin (Shanghai) 37:379-385.

Wang Y, Liang R, Lin J, Chen J, Zhang Q, Li J, Wang M, Hui X, Tan H, Fu Q (2021a) Biodegradable polyurethane nerve guide conduits with different moduli influence axon regeneration in transected peripheral nerve injury. J Mater Chem B 9:7979-7990.

Wang Z, Hu W, Du Y, Xiao Y, Wang X, Zhang S, Wang J, Mao C (2020) Green gas-mediated cross-linking generates biomolecular hydrogels with enhanced strength and excellent hemostasis for wound healing. ACS Appl Mater Interfaces 12:13622-13633.

Wang Z, Hu W, You W, Huang G, Tian W, Huselstein C, Wu CL, Xiao Y, Chen Y, Wang X (2021b) Antibacterial and angiogenic wound dressings for chronic persistent skin injury. Chem Eng J 404:126525.

Wang Z, Ke M, He L, Dong Q, Liang X, Rao J, Ai J, Tian C, Han X, Zhao Y (2021c) Biocompatible and antibacterial soy protein isolate/quaternized chitosan composite sponges for acute upper gastrointestinal hemostasis. Regen Biomater 8:rbab034.

Wu P, Zhao Y, Chen F, Xiao A, Du Q, Dong Q, Ke M, Liang X, Zhou Q, Chen Y (2020) Conductive hydroxyethyl cellulose/soy protein isolate/polyaniline conduits for enhancing peripheral nerve regeneration via electrical stimulation. Front Bioeng Biotechnol 8:709.

Wu YX, Ma H, Wang JL, Qu W (2021) Production of chitosan scaffolds by lyophilization or electrospinning: which is better for peripheral nerve regeneration? Neural Regen Res 16:1093-1098.

Xi F, Liu L, Chen Z, Lin X (2009) One-step construction of reagentless biosensor based on chitosan-carbon nanotubes-nile blue-horseradish peroxidase biocomposite formed by electrodeposition. Talanta 78:1077-1082.

Xue C, Ren H, Zhu H, Gu X, Guo Q, Zhou Y, Huang J, Wang S, Zha G, Gu J, Yang Y, Gu Y, Gu X (2017) Bone marrow mesenchymal stem cell-derived acellular matrix-coated chitosan/silk scaffolds for neural tissue regeneration. J Mater Chem B 5:1246-1257.

Zaminy A, Sayad-Fathi S, Kasmaie FM, Jahromi Z, Zendedel A (2021) Decellularized peripheral nerve grafts by a modified protocol for repair of rat sciatic nerve injury. Neural Regen Res 16:1086-1092.

Zhang Q, Du Q, Zhao Y, Chen F, Wang Z, Zhang Y, Ni H, Deng H, Li Y, Chen Y (2017) Graphene oxide-modified electrospun polyvinyl alcohol nanofibrous scaffolds with potential as skin wound dressings. RSC Adv 7:28826-28836.

Zhao P, Liu H, Deng H, Xiao L, Qin C, Du Y, Shi X (2014) A study of chitosan hydrogel with embedded mesoporous silica nanoparticles loaded by ibuprofen as a dual stimuli-responsive drug release system for surface coating of titanium implants. Colloids Surf B Biointerfaces 123:657-663.

Zhao Y, Liu H, Wang Z, Zhang Q, Li Y, Tian W, Tong Z, Wang Y, Huselstein C, Shi X, Chen Y (2018a) Electrodeposition to construct mechanically robust chitosan-based multi-channel conduits. Colloids Surf B Biointerfaces 163:412-418.

Zhao Y, Wang Z, Zhang Q, Chen F, Yue Z, Zhang T, Deng H, Huselstein C, Anderson DP, Chang PR, Li Y, Chen Y (2018b) Accelerated skin wound healing by soy protein isolate–modified hydroxypropyl chitosan composite films. Int J Biol Macromol 118:1293-1302.

C-Editor: Zhao M; S-Editor: Li CH; L-Editors: Van Deusen A, Li CH, Song LP; T-Editor: Jia Y